

# Subalpine zone delineation using LiDAR and Landsat imagery

Authors:

Hans Ole Ørka<sup>a,\*</sup>, Michael A. Wulder<sup>b</sup>, Terje Gobakken<sup>a</sup> & Erik Næsset<sup>a</sup>

Address:

<sup>a</sup> Norwegian University of Life Sciences, Department of Ecology and Natural Resource Management, P.O. Box 5003, NO-1432 Ås, Norway

<sup>b</sup> Canadian Forest Service (Pacific Forestry Centre), Natural Resources Canada, 506 West Burnside Road, Victoria, Canada BC V8Z 1M5

\* Corresponding author:

Hans Ole Ørka

E-mail address: [hans-ole.orka@umb.no](mailto:hans-ole.orka@umb.no)

Phone: +47 64965799;

Fax: +47 64965802

## Pre-print of published version.

### Reference:

Ørka, H.O., M.A. Wulder, T. Gobakken and E. Næsset. (2012). Subalpine zone delineation using LiDAR and Landsat imagery. Remote Sensing of Environment. Vol. 119, pp. 11-20.

### DOI.

<http://dx.doi.org/10.1016/j.rse.2001.11.023>

### Disclaimer:

The PDF document is a copy of the final version of this manuscript that was subsequently accepted by the journal for publication. The paper has been through peer review, but it has not been subject to any additional copy-editing or journal specific formatting (so will look different from the final version of record, which may be accessed following the DOI above depending on your access situation).

## Abstract

The subalpine zone is the transition between forest and alpine vegetation communities. In Norway, as in many other nations, low productivity or non-merchantable forests, like the subalpine zone, are not routinely subject to inventory programs. Awareness of expected changes in the sub-alpine zone as a result of a warmer climate, and the interest in full carbon accounting at the national level, has dictated a need for data capture in these mountainous areas. We propose an approach for integrating strip samples of Light Detection and Ranging (LiDAR) data with Landsat imagery to delineate the subalpine zone. In the current study the subalpine zone was defined according to international definitions based on tree heights and canopy cover. The three-dimensional measurements of forest structure obtained from LiDAR enable a delineation of the subalpine zone. The approach was implemented using 53 LiDAR sample strips in Hedmark County, Norway, and validated with field measurements at 26 locations. The subalpine zone boundaries were found to be within one Landsat pixel, on average, when validated using an image gradient technique. Furthermore, binomial logistic regression was used to upscale the LiDAR classes to the entire county (27 400 km<sup>2</sup>) using satellite images and information derived from a digital terrain model. The result from the binomial logistic regression was a probability map suitable for monitoring changes in the extent and location of the subalpine zone. The probability surface was separated into hard classes by calibrated alpha-cuts derived using density estimation to support the information needs of inventory stratification and area estimation.

*Keywords:* Subalpine zone; Forest-tundra ecotone; LiDAR; Airborne laser scanning; Satellite data; Landsat; Canopy coverage; Logistic regression; National forest inventory.

## 1. Introduction

The subalpine zone is defined as the transition between the forest and alpine vegetation communities (Kimmins, 1997). Transitions between two different vegetation communities are referred to as ecotones (Clements, 1905). The forest-tundra ecotone is also often understood as analogous to the subalpine zone, with various definitions and terms for this ecotone in usage (c.f. Callaghan et al., 2002; Löve, 1970). However, there is agreement that the subalpine zone is limited downwards by the forest line and upwards by the tree line (Kimmins, 1997). Forest and tree lines are often defined according to tree height ( $h$ ), tree density ( $N$ ) and/or canopy coverage ( $C$ ). The definitions applied in the current study were selected to provide results consistent with those applied in international reporting. The definition of “other wooded land” by the United Nations Food and Agricultural Organization (FAO) was applied for the subalpine zone. Hence, in the current study the subalpine zone is defined as the area where the crown coverage of trees, higher than 5 m, is between 5 and 10 %, or where the joint crown coverage of trees and shrubs, higher than 0.5 m, are larger than 10 % (FAO, 2006).

In a recent meta-analysis it was shown that half of the alpine tree lines included in a global study had advanced during the last century, while only 1% of the studies indicated recession (Harsch et al., 2009). Alpine forest and tree lines are expected to advance as a result of a warmer climate (Dalen & Hofgaard, 2005; Harsch et al., 2009), with changes in human use and activities in mountain areas also expected to affect the subalpine zone e.g. diminished grazing of domestic animals (Cairns & Moen, 2004; Hofgaard, 1997). The ongoing and expected changes in the subalpine zone have increased the demand for information about this ecotone. Changes in the subalpine zone will have an influence on biodiversity, landscape characteristics, biomass, and carbon pools in the zone itself as well as in the adjacent forested and alpine areas. Countries that

have ratified the Kyoto protocol are also committed to report land use change attributable to deforestation, afforestation and reforestation (UNFCCC, 2008). Consequently, there is an urgent need for an updated complete national mapping of the subalpine zone and a capacity to alter the zone boundaries based upon future developments. For instance, there is a burgeoning interest in full carbon accounting requiring inventories and monitoring of low biomass areas such as the subalpine zone. National inventories and monitoring systems have until now typically not included the subalpine zone, as the focus has traditionally been on productive forests with resource management aims. Furthermore, the expenses related to establishing and measuring field plots in remote mountainous areas have further limited the focus on such areas in national inventories. The lack of information on the area and the extent of the subalpine zone results in an inability to report the current state and related monitoring of changes in this ecotone. Hence, National Forest Inventories (NFI) are under pressure to develop protocols to incorporate the need for inventory and monitoring of the subalpine zone.

Remote sensing offers possibilities for mapping and monitoring of large areas. Medium spatial resolution optical satellite images (often defined as a ground sample distance of 10 – 100 meters) have been especially important, providing data with sufficient spatial detail over large areas at sufficiently low costs to meet a range of information needs (Cohen & Goward, 2004; Falkowski et al., 2009). The opening of the United States Geological Survey (USGS) Landsat archive to provide all new and archival data for free (Woodcock et al., 2008) has further accentuated the utility of this data. Landsat data was used to characterize the subalpine zone in Central Siberia (Ranson et al., 2004). Hill et al. (2007) used images from another medium resolution satellite sensor (SPOT 5 HRG) to represent the subalpine zone. Limitations in accuracy obtain with satellite imagery alone have motivated the combination of spectral data from satellite imagery and other spatial data sources (e.g. elevation, climate, soil) (Franklin, 1995; Rogan & Miller, 2007; Wulder et al., 2006). Thematic maps, such as those indicated above, can have limitations in coverage particularly in remote mountainous areas. However, elevation data are often available in these remote areas. Variables derived from elevation may relate to the presence of the subalpine zone (Bader & Ruijten, 2008) and are use to improve maps based upon satellite data (e.g. Wulder et al., 2006). Hence, the combination of medium resolution optical satellite imagery and elevation data (and related derivatives) offers refined potential to map the area and extent of the subalpine zone.

A drawback of medium resolution satellite images is that the spatial resolution often results in a mixture of within pixel vegetation conditions, reducing the capacity to classify beyond broad vegetation types over heterogeneous areas (Wulder, 1998). High spatial resolution remote sensing techniques, including imagery from satellite and airborne platforms and Light Detection and Ranging (LiDAR), provide detailed information about forests and individual trees. However, high acquisition costs make such data unsuitable for large area wall-to-wall inventory and monitoring. To overcome this, high-resolution remotely sensed data may be collected to sample remote areas with either imagery (Falkowski et al., 2009) or LiDAR (Næsset et al., 2009). Comparisons of high spatial resolution imagery and LiDAR remote sensing have shown that LiDAR is among the most promising remote sensing techniques in terms of accuracy of height, volume, and biomass of forested areas (e.g. Hyde et al., 2006; Hyypä & Hyypä, 1999; Lefsky et al., 2001). Furthermore, parameters used to define the forest and tree lines, such as tree height, tree density, and canopy cover, are accurately estimated from LiDAR data (e.g. Hopkinson & Chasmer, 2009; Næsset, 2002, 2009). LiDAR has shown potential for detecting small trees in the subalpine zone (Næsset & Nelson, 2007; Næsset, 2009) and to identify the

forest line (Rees, 2007). Næsset & Nelson (2007) found that 91 % of trees taller than 1 m had positive height measurements by LiDAR, aiding detection of small trees in the subalpine zone. Rees (2007) identified the forest area by extracting LiDAR echoes representing 2 m tall trees with a spacing lower than 10 m between trees. Hence, LiDAR is an attractive data source for identifying the subalpine zone with direct measures, rather than solely empirical, relationships. Hence, delineation of the subalpine zone using LiDAR and without model calibration based on field measurements seems possible and was tested in the current study.

The use of profiling LiDAR as a sampling tool in large area biomass inventories has been proven in many studies (Boudreau et al., 2008; Nelson et al., 2004). Likewise, sampling-based applications utilizing data from airborne scanning LiDAR have recently been demonstrated along with the development of statistical estimators required to yield statistically sound estimates for the area in question (Andersen et al., 2009; Gregoire et al., 2011; Ståhl et al., 2011). The flight lines acquired in such inventories will be continuous and cover forest and bare land as well as the transition zones. Field surveys in such LiDAR based sampling strategies are often mainly based on NFI plots located in the forest area. Hence, by using only the LiDAR measurements to characterize the subalpine zone additional information may be derived without increasing the field survey effort. Furthermore, by combining data from medium resolution satellite images and samples of high spatial resolution LiDAR data the strengths of both sources can be integrated. LiDAR data acquired in a sampling mode provide detailed information on specific locations suitable for extrapolation or model calibration. Furthermore, satellite imagery in combination with elevation data can be deployed to provide full coverage of the region of interest, to provide modeling and extrapolation options, and to support stratification.

The basis for the current study is a framework where a large area inventory is conducted using airborne scanning LiDAR deployed in a strip sampling mode (Næsset et al., 2009). The main objective of the current research was to develop a method combining strip samples of LiDAR with full coverage optical satellite imagery and elevation data to identify the subalpine zone over a large region. The results are intended to increase information regarding the area and location of the subalpine zone without additional field data collection. The specific objectives were to:

- 1) Identify the subalpine zone for specific regions using only LiDAR measurements.
- 2) Model and map the subalpine zone through integration of LiDAR, satellite imagery and elevation data to represent the entire study area of interest.

## **2. Materials and methods**

### **2.1. Study area**

The study area, Hedmark County, is located in southeast Norway (Fig. 1). The total land area of Hedmark is approximately 27 400 km<sup>2</sup>. The county is covered by boreal and alpine vegetation zones with a slightly continental climate (Moen, 1999) . Elevations range from 120 to 2180 m above sea level.

[FIGURE 1]

### **2.2. Field data**

During the summer of 2008 forest and tree lines were mapped in the field at 26 locations in Hedmark County (Fig. 1). Locations were selected subjectively based on the following criteria: co-located with the LiDAR sample transects, availability of orthophotos, accessible for field

work, and spatially distributed over the county. The criteria for selection of field locations were developed in this manner to minimize statistical bias. The subalpine zone was manually delineated by applying common practices following the forest and tree lines in the field. Digitizing was conducted with a commercially available Bluetooth GPS receiver (Holux M-1000) connected to a Personal Data Assistant running Geographical Information System software. Tests of the GPS equipment indicated a positional error of less than 13 m. As shown in Fig. 2, the forest structure and type of forest varies between the field locations. The total length of forest lines digitized in the field was 38.6 km and the length of the tree lines was 42.3 km.

[FIGURE 2]

### **2.3. LiDAR data**

LiDAR data were acquired during the summer of 2006 with the Optech ALTM 3100 laser scanner. Detailed parameters and settings for the acquisitions and sensors are listed in Table 1. Parallel flight lines were flown in an east-west direction with a distance between adjacent flight lines of 6 km. The total length of all flight lines was more than 4500 km and the LiDAR dataset sampled 8.4 % of the study area. The initial processing of the data was accomplished by the contractor (Blom Geomatics, Norway). Planimetric coordinates (in the Universal Transverse Mercator coordinate system (UTM) zone 32 north) and ellipsoidal height values were computed for all echoes. For each acquisition, ground returns were determined using the Terrascan software (Terrasolid Ltd., 2004) and a triangulated irregular network (TIN) was created from the echoes classified as ground returns. Heights above the ground surface were calculated for all echoes by subtracting the respective TIN heights from the height values of all echoes recorded.

[TABLE 1]

### **2.4. Landsat data**

Four different Landsat-5 Thematic Mapper (TM) images were obtained from the USGS to cover the study area. The scenes used were path 197 rows 16 and 18 acquired on 3 June 2007 and path 198 rows 17 and 18 acquired on 10 June 2007. The images were georeferenced using 1:5000 maps and orthorectified using a Digital Terrain Model (DTM) with 25 m pixel size. The images were resampled to the pixel size of the DTM during orthorectification. The error from orthorectification of all four images was less than 1/3 pixel. The orthorectified images were converted to top of atmospheric reflectance (TOA) by the procedure communicated by Han et al. (2007). The TOA corrections account for differences in viewing geometry and sensor configuration. However, variations in absolute atmospheric conditions between images were not corrected. The TOA corrected images were mosaiced together. From the TOA corrected Landsat mosaic the normalized difference vegetation index (NDVI) and the brightness, greenness and wetness from the tassell cap transformation were derived and used (Crist & Kauth, 1986; Huang et al., 2002; Kauth & Thomas, 1976).

### **2.5. Elevation data**

Elevation data were supplied by the Norwegian Mapping Authority as a DTM with 25m pixel size. From the DTM, elevation, slope, solar radiation and curvature were derived and utilized. Slope was computed for each raster cell in the DTM using the average maximum technique on a fitted plane to a 3 × 3 cell neighborhood (Burrough & McDonell, 1998). Global solar radiation in

watt hours per square meter ( $\text{WH m}^{-2}$ ) was computed using the DTM in accordance with Fu and Rich (1999). Curvature describes the shape of the terrain and was computed in a  $3 \times 3$  cell neighborhood (Moore et al., 1991; Zevenbergen & Thorne, 1987). In addition, the location (latitude and longitude) of the pixels was used in the modeling.

## 2.6. Procedure for delineating the subalpine zone

Fig. 3 outlines the implemented procedure for obtaining the full coverage map of the subalpine zone. The flow chart introduces the input data described above, two processing steps and the accuracy assessment in separate light grey boxes. During Step 1, the procedure identifies cover types, forest, alpine and subalpine areas in the LiDAR data, using a rule-based classification. Step 2 describes the integration of LiDAR, satellite imagery and elevation data to define the probability of forest and identification of alpha-cuts to produce a map with hard classes i.e. the cover types; forest, alpine and subalpine. Lastly, the accuracy of both the LiDAR derived classes in step 1 and the full coverage map produced in step 2 was assessed. The two processing steps and the accuracy assessment are described in further detail below.

[FIGURE 3]

### 2.6.1. Identify the subalpine zone using LiDAR data (Step 1)

A classification procedure for automatically assigning cover type based on the LiDAR data was developed. The point cloud obtained from LiDAR sensors can be viewed as a sample of the forest canopy where each echo ( $x, y, z$  – point) is a sample point. Classifying each point according to presence or absence of canopy makes the point cloud a point sample, from which the canopy cover can be estimated as the number of echoes in the canopy over the total number of echoes:

$$C = \frac{N_c}{N_t} \quad (1)$$

where  $C$  is canopy cover,  $N_c$  is number of first returns in canopy, and  $N_t$  is total number of first returns. Similar approaches have frequently been used (c.f. Hopkinson & Chasmer, 2009). Canopy hits were defined based on a height threshold on the LiDAR measured surface height (height above ground). One height threshold was used for defining tree canopy ( $HT_{trees}$ ) and one threshold was used for defining shrubs and trees ( $HT_{shrub+trees}$ ). The height thresholds were used to classify canopy returns ( $N_c$ ) in Eq. 1. The canopy thresholds were set in accordance with the heights in the FAO definitions ( $HT_{trees} = 5$  m and  $HT_{shrub+trees} = 0.5$  m). Hence, canopy cover for trees ( $C_{trees}$ ) was computed as the number of first returns above 5 m divided by the total number of first returns. Canopy cover for trees and shrubs ( $C_{shrub+trees}$ ) was computed as the number of first returns above 0.5 m divided by the total number of first returns. Then the classes, recall as forest, alpine or subalpine zone, were assigned according to this pseudo code:

```

if( $C_{trees} > CT_1$ )
    class = forest
else
    if( $C_{trees} > CT_2$  or  $C_{shrub+trees} > CT_1$ )
        class = subalpine zone

```

```

else
    class = alpine

```

where  $CT_1$  and  $CT_2$  represent the two different canopy cover thresholds. The canopy cover thresholds used to assign classes were  $CT_1 = 0.10$  and  $CT_2 = 0.05$  which correspond to the canopy coverage values in the FAO definitions of forest and other wooded land.

### 2.6.2. Model and map the subalpine zone using full coverage data (Step 2)

Ecotones, like the subalpine zone, are by definition a mixture of two classes, in this case forest and alpine. Soft classifiers are shown to provide a better representation of the vegetation class composition in ecotones than hard classes (Foody, 1996). Binomial logistic regression is widely used in the remote sensing community as a soft classifier because it does not assume a specific distribution regarding the input variables (e.g. Wulder et al., 2006). To predict the appearance of the subalpine zone based on the satellite imagery and elevation data, a binomial logistic regression was estimated in the current study (Eq. 2). The spectral indices (NDVI, brightness, wetness, and greenness), elevation, slope, solar radiation, curvature, and location variables (latitude and longitude) were candidate variables in the estimation. The initial model including all candidate variables was of the form:

$$\log\left(\frac{\pi(\text{FOREST})}{1 - \pi(\text{FOREST})}\right) = \beta_0 + \beta_1 x_1 + \dots + \beta_k x_k \quad (2)$$

where  $\pi(\text{FOREST})$  is the probability of a pixel being forest,  $\beta_0, \beta_1 - \beta_k$  are fixed parameters and  $x_1 - x_k$  are the variables used. Variable selection was conducted using a manual backward elimination process. In addition, highly correlated variables were identified using Person-correlation coefficients and removed so no variables had a higher correlation than 0.50. The reference data included plots of size 625 m<sup>2</sup>, equal to pixel size, laid out with three kilometer spacing along the LiDAR transects. Reference data were stratified as potential subalpine zone area using the DTM. The elevation range of potential subalpine zone area was set to be between 675 and 1150 m above sea level based on local knowledge and photointerpretation. A total of 534 reference plots, where the LiDAR derived cover type was forest or alpine, were used in the binomial logistic regression. The reference plots where the LiDAR derived cover type was subalpine zone were not used in the binomial logistic regression. The fit of the final model was evaluated with Naglekerkes  $R^2$  (Nagelkerke, 1991), the model deviance and the Hosmer-Lemeshows goodness-of-fit test (Hosmer et al., 1997).

The final binomial logistic regression model was used to predict a probability surface in the potential subalpine area in Hedmark, whereby the output surface indicates the probability of a pixel being forest. Even though ecotones are best represented by probability surfaces, a hard classification is often needed when presenting thematic maps of the subalpine zone or when information will be used in international reporting (Hill et al., 2007). Hill et al. (2007) tested two approaches to present the probability surface as a thematic map using alpha-cuts. In the current study we used the probability of forest for the reference plots, estimated by the binomial logistic regression model and probability density functions to identify alpha-cuts. Separate density functions were estimated for the three cover types (forest, alpine and subalpine) using a Gaussian kernel and bandwidth of 0.05 (R Development Core Team, 2009). Then the alpha-cuts were set

for the upper and lower boundaries where the subalpine zone according to the density functions had a higher density than forest and alpine areas.

### 2.6.3. Accuracy assessment

The accuracy of the LiDAR derived cover type classes was validated against the field measured forest and tree lines. The cover type classes (forest, alpine, subalpine zone) determined using LiDAR data and the approach described above at the 26 field locations was assessed by utilizing an image gradient method (Pitas, 2000; Wulder et al., 2007). The image gradient describing the rate of change in cover type class in a local neighborhood was computed as:

$$|\nabla f(x,y)| = \sqrt{[f(x+1,y) - f(x,y)]^2 + [f(x,y+1) - f(x,y)]^2} \quad (3)$$

where  $|\nabla f(x,y)|$  is the gradient and  $x$  and  $y$  are row and column in the raster file created at each location. The image gradient map has large values where the cover type classes change between neighboring pixels and values of zero where they do not change. Furthermore, the image gradient values were aggregated for different distances in pixels to the field measured lines and averaged over all field locations. Hence, the average change between pixels located at different distances from the field measured forest and tree lines are computed and analyzed. The largest values indicate the strongest gradient or highest rate of change in classes between pixels and appear where the field measured forest and tree lines are located.

The current study utilized tree heights and canopy cover derived directly from LiDAR data. However, these variables are only proxies for the real values since a LiDAR pulse will always penetrate into the canopy before an echo is triggered (Gaveau & Hill, 2003; Ørka et al., 2010). In previous studies, canopy cover has been derived for measurements above a certain height threshold often equal to the height where reference data were collected, such as with a hemispheric camera (e.g. Riano et al., 2004). The current study used height thresholds of 0.5 and 5 m, for shrubs and trees, respectively, which is in accordance with international forest definitions. In order to evaluate if the chosen canopy cover and height thresholds in the classification of the LiDAR data was appropriate, a sensitivity analysis was conducted. Different height thresholds ( $HT_{trees} = \{2, 2.5, \dots, 9.5, 10 \text{ m}\}$  and  $HT_{shrub+trees} = \{0.25, 0.30, \dots, 0.95, 1 \text{ m}\}$ ) and canopy coverage thresholds ( $CT_1 = \{0.055, 0.060, \dots, 0.195, 0.20\}$  and  $CT_2 = \{0.005, 0.010, \dots, 0.145, 0.15\}$ ) were tested. The mean gradient value at the forest and tree line were recorded for every combination of height and canopy cover thresholds. In addition, the number of pixels from the peak of the image gradient to the field measured line was evaluated for both the forest and tree line.

The logistic regression model and the alpha-cut were validated using a test dataset which covered the plots located  $\pm 1$  km in the east – west direction of the calibration plots and located inside the potential subalpine zone area. The test dataset plots were classified according to Step 1 (Section 2.6.1). The classification accuracy of the binomial logistic regression model and alpha-cuts was validated both for the calibration and the test datasets.

## 3. Results

### 3.1. Accuracy of LiDAR cover type classification

The predicted forest and tree lines showed a good correspondence with the field measured lines (Fig. 4). The average image gradient values peaked at the location of field measured lines. Consequently, the classification of the LiDAR data shifts most frequently between pixels near

the field measured lines. The high gradient values below the field measured forest line reflect the patchiness of the forest near the forest line (Fig. 4). In the subalpine zone and in the alpine area the gradient values are low. Hence, the vegetation above the forest line appears more homogeneous as classified by LiDAR data. A visual inspection of all the field locations indicated that four field measured forest lines (15.4 %) and two tree lines (7.7 %) did not have a satisfactory match of field measured and LiDAR derived boundaries of the subalpine zone. Examples from three of the 26 field locations illustrating accuracy and errors of the LiDAR cover type classification appear in Fig. 5.

The sensitivity analysis presented in Fig. 6 demonstrates that the accuracy obtained was indifferent to the selection of height and canopy cover thresholds. The difference between highest image gradient value and the field measured lines was within plus or minus one pixel (50 m) for many combinations of height- and canopy cover thresholds. However, the selected height and canopy thresholds corresponding to the FAO definitions were close to the highest average image gradient values as illustrated with the dashed lines in the contour plots in Fig. 6. Higher values could be obtained by reducing the height threshold slightly. Minor changes in the canopy coverage thresholds, e.g. by 0.01 units, did not affect the accuracy at all.

[FIGURE 4]

[FIGURE 5]

[FIGURE 6]

### 3.2. Accuracy of subalpine zone delineation using full coverage data

The selected variables and fit statistics for the estimated binomial logistic regression model are presented in Table 2. The two Landsat variables greenness and NDVI were highly correlated ( $r = 0.85$ ). During the modeling NDVI was selected because of better models obtained compared to using greenness. We included both NDVI and brightness because of the significant contribution of both indices to the model. The elevation and slope variables derived from the digital terrain model were strong explanatory variables. However, neither the solar radiation nor the curvature provided additional information. Wetness and longitude were significant variables in the model following a backward elimination procedure ( $0.05 > p > 0.01$ ). However, the variables were removed to get a simpler model without an essential reduction in Akaike information criterion (AIC). The Hosmer and Lemeshow statistics (Hosmer et al., 1997) indicated that the final model fit the data sufficiently well ( $p = 0.40$ ). The proportion of variation explained by the model expressed by Nagelkerke's  $R^2$  was 0.73.

Alpha-cuts were selected according to the probability density functions estimated for the three cover type classes (Fig. 7). The crossing of the subalpine and alpine density functions in Fig. 7 resulted in a lower alpha-cut of 0.16 and the crossing of forest and subalpine resulted in an upper alpha-cut of 0.79. Hence, pixels having a probability of forest between 0.16 and 0.79 were classified as subalpine zone. The selected alpha-cuts resulted in an overall classification accuracy of 68.8 % and a kappa value of 0.52. For the subalpine zone cover type the producer's accuracy was 56.6% and the user's accuracy 32.5%. The error matrix for the calibration and the test data sets appear in Table 3.

Predicting the probabilities for every pixel in the county belonging to the potential subalpine zone area (See section 2.6.2.) and assigning classes to the pixels based on the estimated alpha-cut values resulted in a map of the subalpine zone in Hedmark with a total area of 3660 km<sup>2</sup>, representing 14% of the land area in Hedmark.

[TABLE 2]  
[FIGURE 7]  
[TABLE 3]

## 4. Discussion

### 4.1. LiDAR cover type classification

The current study utilized tree heights and canopy cover derived directly from LiDAR data to classify cover types. However, these variables are only proxies for the real values since a LiDAR pulse will always penetrate into the canopy before an echo is triggered (Gaveau & Hill, 2003; Ørka et al., 2010). In addition, different LiDAR sensors and acquisition settings affect the LiDAR measurements of forest canopies (Chasmer et al., 2006; Næsset, 2009; Ørka et al., 2010). In another subalpine area in Norway tree height underestimation compared to true tree height was in the range of 0.35 – 1.47 m (Næsset, 2009). The underestimation in the study by Næsset (2009) was affected by sensor and acquisition settings together with tree species and the terrain model. The sensitivity analysis performed in the current study suggest that penetration of LiDAR echoes into the canopy was present in the current dataset, since the accuracy of both forest and tree lines was slightly improved in the LiDAR classification with height threshold slightly lower than those specified by the definitions. In previous studies, canopy cover has been derived for measurements above a certain height threshold often equal to the height where reference data were collected with e.g. hemispheric camera (e.g. Riano et al., 2004). Changing the canopy coverage thresholds in the sensitivity analysis did not increase the accuracy of the classification. Differences in measurements obtained with different sensors and acquisitions usually necessitate field data for properly calibration of models. The sensitivity analysis suggests that the effect of varying sensors and acquisition parameters would have a minor impact on the LiDAR classification but, further research would be required to confirm this.

When mapping the forest and tree lines in the field the uppermost line was followed. Hence, there could be areas with lower density of trees or lower tree heights below the mapped areas. In Fig. 5, the site at Litbutjønn illustrates such a case. In the south there are areas matching the criteria of the subalpine zone about 100 meters after an open/alpine area. When following the tree line to the north the tree density slightly decreased and thus an error was made when mapping the tree line in field. At the Danseren site, only minor errors were introduced by following the forest line. The third location in Fig. 5, Tittelsjøen, the LiDAR derived forest line was effected by the species composition at the location. At Tittelsjøen, the tree line is abrupt and formed by birch and was well delineated with the classification of LiDAR data. The forest line is diffuse and comprised of spruce trees. The spruce trees have a conical form and hence the canopy cover at the base is much greater than the canopy coverage at 5 m. LiDAR derived canopy coverage will therefore underestimate true canopy coverage significantly at that spruce dominated site. Estimation of canopy coverage with a field calibrated and species specific model might have provided a better estimate of the forest line at this location.

### 4.2. Subalpine zone delineation using full coverage data

The binomial logistic regression model developed included five variables important for characterizing the subalpine zone in Hedmark. Two Landsat derived variables were used in the model, NDVI and brightness. The two variables describe different vegetation (NDVI) and non-vegetation (brightness) properties. The probability of forest increases when NDVI increases and

brightness decreases. For the DTM derived attributes, elevation and slope were important. Higher elevations reduce the probability of forest. Furthermore, increasing slope increase the probability for forest. In Hedmark one often sees forest growing on the slopes of valleys and when the terrain flatten out toward the peak forest growth is limited because of higher exposure to weather conditions. Even though solar radiation and topographic position illustrated by curvature were expected to be important for tree growth, these variables were not statistically significant. In a study in the tropical Andes, elevation, aspect and a compound topographic index were significant when estimating the probability of forest (Bader & Ruijten, 2008). The only common variable with the current study and the study by Bader and Ruijten (2008) was elevation, which indicates the importance of elevation as an overall driving factor for forest and tree lines.

The accuracy (overall accuracy = 69% and kappa = 0.52) obtained for classification with the binomial logistic regression model and alpha-cuts was lower than what is reported in many land cover classification studies, for example the land cover projects in North-America, the National Land Cover Database in United States (Homer et al., 2007) and the Earth Observation for Sustainable Developments of Forests in Canada (Wulder et al., 2008). However, Wilkinson (2005) analyzed the accuracies of over 500 peer-reviewed land cover classification experiment carried out over 15 years and reported that the average overall accuracy was 76% (with a standard deviation of 15.6%) and average kappa was 0.65 (with a standard deviation of 0.20). Hence, the accuracy obtained in the current study is within one standard deviation of the average accuracies obtained in land cover classification reported by Wilkinson (2005). This accuracy was obtained despite the high degree of mixing with the subalpine zone and the two adjacent classes, the forest and alpine classes (Table 3). Because of the high mixing we consider the total classification measures, overall accuracy and kappa coefficient, to be most important. Furthermore, when considering the high degree of mixing present, the obtained accuracy was considered acceptable for area estimation and monitoring transitions over large areas, especially since the pure forest and alpine classes were identified with high accuracies.

In the current study, only the alpine transition zones were mapped in field. However, the classification of LiDAR data did not distinguish between forest-alpine transitions and other forest – non-forest transitions inside the potential area for the subalpine zone. Hence, the areas below the forest zone will include other transitions zones and also non-forested areas (Fig. 4). Transitions occurring in the forest may consist of mountain peat lands or transitions related to change in nutrient level, e.g. from deep soils to bare rock. Hence, enhancement considering additional land cover classes could be implemented to improve the separation of these transitions.

#### **4.3. Application for subalpine mapping and monitoring**

In this study, the subalpine zone in Hedmark County, Norway was successfully mapped. The approach presented utilized high spatial resolution LiDAR data sampled for parts of the county. Classification of the LiDAR data enabled accurate depiction of the subalpine zone over a large geographical area without calibration based on field measurements. The information derived from LiDAR data was combined with Landsat and elevation data to produce full coverage maps of the subalpine zone. Collecting expensive field data from remote mountainous areas is not needed using this method. An improved capacity for the national forest inventory to capture the entire forested area, rather than limited to managed forest areas at lower elevations, is increasingly desired and may be aided by the approach presented here. The ability to portray

transitional areas enhances our ability to facilitate stratification and to monitor and report on carbon stocks and change and to ensure that all relevant forested areas are included. Studies of climate change may also be aided by the ability to map the subalpine zone over large areas. Hence, changes in the subalpine zone can be monitored over vast areas and not only at specific sites. Changes found over time will be important for describing the change processes and the rates of transition among cover types.

The products from the current study are important in monitoring areas in the subalpine zone. Maps of changes in the subalpine zone over time can be combined with information about human activity or grazing by animals to separate the response of climate change on the tree lines from effects of land use change. As pointed out by Hill et al. (2007), hard classifications of ecotones are often needed for map products. Hill et al. (2007) used two different approaches to produce alpha-cuts used to divide the subalpine zone into classes. In the current study a new method for dividing the probability surface into hard classes was presented. As opposed to the methods presented by Hill et al. (2007), our method uses information about ecotone derived using LiDAR to produce these alpha-cuts. The proposed method produces a hard classification from which an estimate of the area of the subalpine zone can be derived. The method described also has a probability surface as one of its products. Probability surfaces, or outcomes from soft classifiers, are more robust in monitoring and change detection in transition zones (Foody, 2001). In the alpine environment, it has been reported that diffuse tree lines are more likely to have advanced into the alpine areas than other tree lines types (Harsch et al., 2009). The key research outcomes include, that monitoring of the subalpine zone is best done using the probability map, and that the classified map provides area estimates and offers a support for area-wide attribute estimation (e.g., biomass) using LiDAR-assisted inventory procedures such as those proposed by Næsset et al. (2009).

## **5. Conclusions**

The current study demonstrates that a national and regional forest inventory utilizing scanning LiDAR operated as a strip sampling tool (Næsset et al., 2009) and additional remotely sensed data can derive the area of the subalpine zone or other transitional areas at a regional scale, without increasing field inventory intensity. The method for delineating the subalpine zone using samples of LiDAR data is simple and straightforward. The use of logistic regression and alpha-cut calibrated with LiDAR data using a density estimation approach provide a hard classification for map products, area estimation and stratification. The probability map is suitable for monitoring purposes. If detailed monitoring is requested, for example monitoring of regeneration, growth, and mortality of single trees, then methods utilizing field calibration based on a statistically sound sample of ground data are required. As, the statistical framework for utilizing strip samples of LiDAR develops and become operational the approach presented here would provide additional information of transitional areas also other than the subalpine zone. Furthermore, the approach presented could be modified and extended to map also other areas.

## **Acknowledgements**

This research was funded by the Norwegian University of Life Sciences and the Research Council of Norway (research grant #192792/I99) and is a contribution to the NORKLIMA project entitled “Effects of changing climate on the alpine tree line and mountain forest carbon pools along 1500 km n-s and elevation gradients” (research grant #184636/S30). We also wish to

thank Blom Geomatics, Norway, for providing and processing the LiDAR data and one anonymous reviewer for comments on the manuscript.

## References

- Andersen, H.-E., Barrett, T., Winterberger, K., Strunk, J., & Temesgen, H. (2009). Estimating forest biomass on the western lowlands of the Kenai Peninsula of Alaska using airborne lidar and field plot data in a model-assisted sampling design. In, *IUFRO Div. 4 Symposium, Extending Forest Inventory and Monitoring* (p. 5). Québec City, Quebec, Canada
- Bader, M.Y., & Ruijten, J.J.A. (2008). A topography-based model of forest cover at the alpine tree line in the tropical Andes. *Journal of Biogeography*, 35, 711-723.
- Baltsavias, E.P. (1999). Airborne laser scanning: basic relations and formulas. *ISPRS Journal of Photogrammetry and Remote Sensing*, 54, 199-214.
- Boudreau, J., Nelson, R.F., Margolis, H.A., Beaudoin, A., Guindon, L., & Kimes, D.S. (2008). Regional aboveground forest biomass using airborne and spaceborne LiDAR in Quebec. *Remote Sensing of Environment*, 112, 3876-3890.
- Burrough, P.A., & McDonell, R.A. (1998). *Principles of Geographical Information Systems*. New York: Oxford University Press.
- Cairns, D.M., & Moen, J. (2004). Herbivory Influences Tree Lines. *Journal of Ecology*, 92, 1019-1024.
- Callaghan, T.V., Werkman, B.R., & Crawford, R.M.M. (2002). The tundra-taiga interface and its dynamics: Concepts and applications. *Ambio*, 6-14.
- Chasmer, L., Hopkinson, C., Smith, B., & Treitz, P. (2006). Examining the influence of changing laser pulse repetition frequencies on conifer forest canopy returns. *Photogrammetric Engineering and Remote Sensing*, 72, 1359-1367.
- Clements, F.E. (1905). *Research methods in ecology*. Lincoln, Neb.: University Publishing Company.
- Cohen, W.B., & Goward, S.N. (2004). Landsat's role in ecological applications of remote sensing. *Bioscience*, 54, 535-545.
- Crist, E.P., & Kauth, R.J. (1986). The Tasseled Cap de-mystified (transformations of MSS and TM data). *Photogrammetric Engineering and Remote Sensing*, 52, 81-86.
- Dalen, L., & Hofgaard, A. (2005). Differential regional treeline dynamics in the Scandes Mountains. *Arctic Antarctic and Alpine Research*, 37, 284-296.
- Falkowski, M.J., Wulder, M.A., White, J.C., & Gillis, M.D. (2009). Supporting large-area, sample-based forest inventories with very high spatial resolution satellite imagery. *Progress in Physical Geography*, 33, 403-423.

- 557 FAO (2006). Global Forest Resources Assessment 2005 - Progress towards sustainable forest  
558 management. In, *FAO Forestry Paper 147*. Rome: Food and Agriculture Organization of the  
559 United Nations.
- 560 Foody, G.M. (1996). Fuzzy modelling of vegetation from remotely sensed imagery. *Ecological*  
561 *Modelling*, 85, 3-12.
- 562 Foody, G.M. (2001). Monitoring the magnitude of land-cover change around the southern limits  
563 of the Sahara. *Photogrammetric Engineering and Remote Sensing*, 67, 841-848.
- 564 Franklin, J. (1995). Predictive vegetation mapping: geographic modelling of biospatial patterns  
565 in relation to environmental gradients. *Progress in Physical Geography*, 19, 474.
- 566 Fu, P., & Rich, P.M. (1999). Design and implementation of the Solar Analyst: an ArcView  
567 extension for modeling solar radiation at landscape scales. In, *Proceedings of the 19th Annual*  
568 *ESRI User Conference*. San Diego, USA: ESRI.
- 569 Gaveau, D.L.A., & Hill, R.A. (2003). Quantifying canopy height underestimation by laser pulse  
570 penetration in small-footprint airborne laser scanning data. *Canadian Journal of Remote Sensing*,  
571 29, 650-657.
- 572 Gregoire, T., Ståhl, G., Næsset, E., Gobakken, T., Nelson, R., & Holm, S. (2011). Model-assisted  
573 estimation of biomass in a LiDAR sample survey in Hedmark county, Norway. *Canadian*  
574 *journal of forest research-Revue canadienne de recherche forestier*, 41, 83-95.
- 575 Han, T., Wulder, M.A., White, J.C., Coops, N.C., Alvarez, M.F., & Butson, C. (2007). An  
576 Efficient Protocol to Process Landsat Images for Change Detection With Tasselled Cap  
577 Transformation. *Geoscience and Remote Sensing Letters*, 4, 147-151.
- 578 Harsch, M., A., Hulme, P., E., McGlone, M., S., & Duncan, R., P. (2009). Are treelines  
579 advancing? A global meta-analysis of treeline response to climate warming. *Ecology Letters*, 12,  
580 1040-1049.
- 581 Hill, R.A., Granica, K., Smith, G.M., & Schardt, M. (2007). Representation of an alpine treeline  
582 ecotone in SPOT 5 HRG data. *Remote Sensing of Environment*, 110, 458-467.
- 583 Hofgaard, A. (1997). Inter-Relationships between Treeline Position, Species Diversity, Land Use  
584 and Climate Change in the Central Scandes Mountains of Norway. *Global Ecology and*  
585 *Biogeography Letters*, 6, 419-429.
- 586 Homer, C., Dewitz, J., Fry, J., Coan, M., Hossain, N., Larson, C., Herold, N., McKerrow, A.,  
587 VanDriel, J.N., & Wickham, J. (2007). Completion of the 2001 National Land Cover Database  
588 for the conterminous United States. *Photogrammetric Engineering and Remote Sensing*, 73, 337-  
589 341.
- 590 Hopkinson, C., & Chasmer, L. (2009). Testing LiDAR models of fractional cover across  
591 multiple forest ecozones. *Remote Sensing of Environment*, 113, 275-288.

592 Hosmer, D.W., Hosmer, T., le Cessie, S., & Lemeshow, S. (1997). A comparison of goodness-  
593 of-fit tests for the logistic regression model. *Statistics in Medicine*, 16, 965-980.

594 Huang, C., Wylie, B., Yang, L., Homer, C., & Zylstra, G. (2002). Derivation of a tasseled cap  
595 transformation based on Landsat 7 at-satellite reflectance. *International Journal of Remote*  
596 *Sensing*, 23, 1741-1748.

597 Hyde, P., Dubayah, R., Walker, W., Blair, J.B., Hofton, M., & Hunsaker, C. (2006). Mapping  
598 forest structure for wildlife habitat analysis using multi-sensor (LiDAR, SAR/InSAR, ETM+ ,  
599 Quickbird) synergy. *Remote Sensing of Environment*, 102, 63-73.

600 Hyypä, H., & Hyypä, J. (1999). Comparing the accuracy of laser scanner with other optical  
601 remote sensing data sources for stand attributes retrieval. *The Photogrammetric Journal of*  
602 *Finland*, 16, 5 -15.

603 Kauth, R.J., & Thomas, G.S. (1976). The tasseled cap—a graphic description of the spectral-  
604 temporal development of agricultural crops as seen by Landsat. In, *Final proceedings: 2nd*  
605 *international symposium on machine processing of remotely sensed data*. West Lafayette, India:  
606 Purdue University.

607 Kimmins, J.P. (1997). *Forest Ecology, A foundation for sustainable management*, 2nd ed. Upper  
608 Saddle River, New Jersey: Prentice-Hall Inc.

609 Lefsky, M.A., Cohen, W.B., & Spies, T.A. (2001). An evaluation of alternate remote sensing  
610 products for forest inventory, monitoring, and mapping of Douglas-fir forests in western Oregon.  
611 *Canadian Journal of Forest Research-Revue Canadienne De Recherche Forestiere*, 31, 78-87.

612 Löve, D. (1970). Subarctic and Subalpine: Where and What? *Arctic and Alpine Research*, 2, 63-  
613 73.

614 Moen, A. (1999). *National atlas of Norway: Vegetation*. Hønefoss: Norwegian Mapping  
615 Authority, Hønefoss.

616 Moore, I.D., Grayson, R.B., & Landson, A.R. (1991). Digital Terrain Modelling: A Review of  
617 Hydrological, Geomorphological, and Biological Applications. *Hydrological Processes*, 5, 3–30.

618 Næsset, E. (2002). Predicting forest stand characteristics with airborne scanning laser using a  
619 practical two-stage procedure and field data. *Remote Sensing of Environment*, 80, 88-99.

620 Næsset, E., & Nelson, R. (2007). Using airborne laser scanning to monitor tree migration in the  
621 boreal-alpine transition zone. *Remote Sensing of Environment*, 110, 357-369.

622 Næsset, E. (2009). Influence of terrain model smoothing and flight and sensor configurations on  
623 detection of small pioneer trees in the boreal-alpine transition zone utilizing height metrics  
624 derived from airborne scanning lasers. *Remote Sensing of Environment*, 113, 2210-2223.

625 Næsset, E., Gobakken, T., & Nelson, R. (2009). Sampling and mapping forest volume and  
626 biomass using airborne LIDARs. *Proceedings of the Eight Annual Forest Inventory and Analysis*  
627 *Symposium, Monterey, CA, USA*, 297-301.

628 Nagelkerke, N.J.D. (1991). A note on a general definition of the coefficient of determination.  
629 *Biometrika*, 78, 691-692.

630 Nelson, R., Short, A., & Valenti, M. (2004). Measuring biomass and carbon in Delaware using  
631 an airborne profiling LIDAR. *Scandinavian Journal of Forest Research*, 19, 500-511.

632 Ørka, H.O., Næsset, E., & Bollandsås, O.M. (2010). Effects of different sensors and leaf-on and  
633 leaf-off canopy conditions on echo distributions and individual tree properties derived from  
634 airborne laser scanning. *Remote Sensing of Environment*, 114, 1445-1461.

635 Pitas, I. (2000). *Digital image processing algorithms and applications*. New York: Wiley.

636 R Development Core Team (2009). *R: A Language and Environment for Statistical Computing*.  
637 Vienna, Austria.: R Foundation for Statistical Computing.

638 Ranson, K.J., Sun, G., Kharuk, V.I., & Kovacs, K. (2004). Assessing tundra-taiga boundary with  
639 multi-sensor satellite data. *Remote Sensing of Environment*, 93, 283-295.

640 Rees, W.G. (2007). Characterisation of Arctic treelines by LiDAR and multispectral imagery.  
641 *Polar Record*, 43, 345-352.

642 Riano, D., Valladares, F., Condes, S., & Chuvieco, E. (2004). Estimation of leaf area index and  
643 covered ground from airborne laser scanner (Lidar) in two contrasting forests. *Agricultural and*  
644 *Forest Meteorology*, 124, 269-275.

645 Rogan, J., & Miller, J. (2007). Integrating GIS and remotely sensed data for mapping forest  
646 disturbance and change. In M.A. Wulder & S.E. Franklin (Eds.), *Understanding forest*  
647 *disturbance and spatial pattern* (pp. 133-171). Boca Raton, FL, USA: CRC Taylor & Francis.

648 Ståhl, G., Holm, S., Gregoire, T., Gobakken, T., Næsset, E., & Nelson, R. (2011). Model-based  
649 inference for biomass estimation in a LiDAR sample survey in the county of Hedmark County,  
650 Norway. *Canadian journal of forest research-Revue canadienne de recherche forestier*, 41, 96-  
651 107.

652 UNFCCC (2008). *Kyoto protocol reference manual on accounting of emissions and assigned*  
653 *amount*

654 Wilkinson, G.G. (2005). Results and implications of a study of fifteen years of satellite image  
655 classification experiments. *IEEE Transactions on Geoscience and Remote Sensing*, 43, 433-440.

656 Woodcock, C., Allen, R., Anderson, M., Belward, A., Bindschadler, R., Cohen, W., Gao, F.,  
657 Goward, S., Helder, D., & Helmer, E. (2008). Free access to Landsat imagery. *Science*, 320,  
658 1011.

- 659     Wulder, M. (1998). Optical remote-sensing techniques for the assessment of forest inventory and  
660     biophysical parameters. *Progress in Physical Geography*, 22, 449-476.
- 661     Wulder, M.A., White, J.C., Bentz, B., Alvarez, M.F., & Coops, N.C. (2006). Estimating the  
662     probability of mountain pine beetle red-attack damage. *Remote Sensing of Environment*, 101,  
663     150-166.
- 664     Wulder, M.A., Han, T., White, J.C., Butson, C.R., & Hall, R.J. (2007). An approach for edge  
665     matching large-area satellite image classifications. *Canadian Journal of Remote Sensing*, 33,  
666     266-277.
- 667     Wulder, M.A., White, J.C., Cranny, M., Hall, R.J., Luther, J.E., Beaudoin, A., Goodenough,  
668     D.G., & Dechka, J.A. (2008). Monitoring Canada's forests. Part 1: Completion of the EOSD land  
669     cover project. *Canadian Journal of Remote Sensing*, 34, 549-562.
- 670     Zeverbergen, L.W., & Thorne, C.R. (1987). Quantitative Analysis of Land Surface Topography.  
671     *Earth Surface Processes and Landforms*, 12, 47-56.  
672

673 **Table 1**

674 Table 1. Sensors and acquisition settings

Parameters	
Platform	PA31 Piper Navajo
Sensor	ALTM 3100
Mean flying altitude above ground (m)	800
Pulse repetition frequency (kHz)	100
Scan frequency (Hz)	55
Half scan angle (deg.)	17
Mean flying speed ( $\text{ms}^{-1}$ )	ca. 75
Mean pulse density ( $\text{m}^{-2}$ )	2.7 <sup>a</sup>
Beam divergence (mrad)	0.26
Footprint diameter (cm)	21 <sup>a</sup>

675 <sup>a</sup>Computed after Baltsavias (1999) based on mean acquisition settings.

676

677

678 **Table 2**

679 Table 2. Parameters and fit statistics for the logistic regression model.

Coefficient	Estimate	Z	p-value
Intercept	4.09	2.56	0.010
NDVI	17.83	8.60	0.000
Brightness	-19.97	-6.38	0.000
Elevation	-0.01	-5.93	0.000
Slope	0.10	3.33	0.001
Latitude	0.01	3.54	0.000
Model fit:			
Hosmer-Lemeshow goodness of fit <sup>a</sup>		-0.85	0.397
Deviance test			1

680 <sup>a</sup>Hosmer-Lemeshow goodness of fit (Hosmer et al., 1997)

681

682

683 **Table 3**

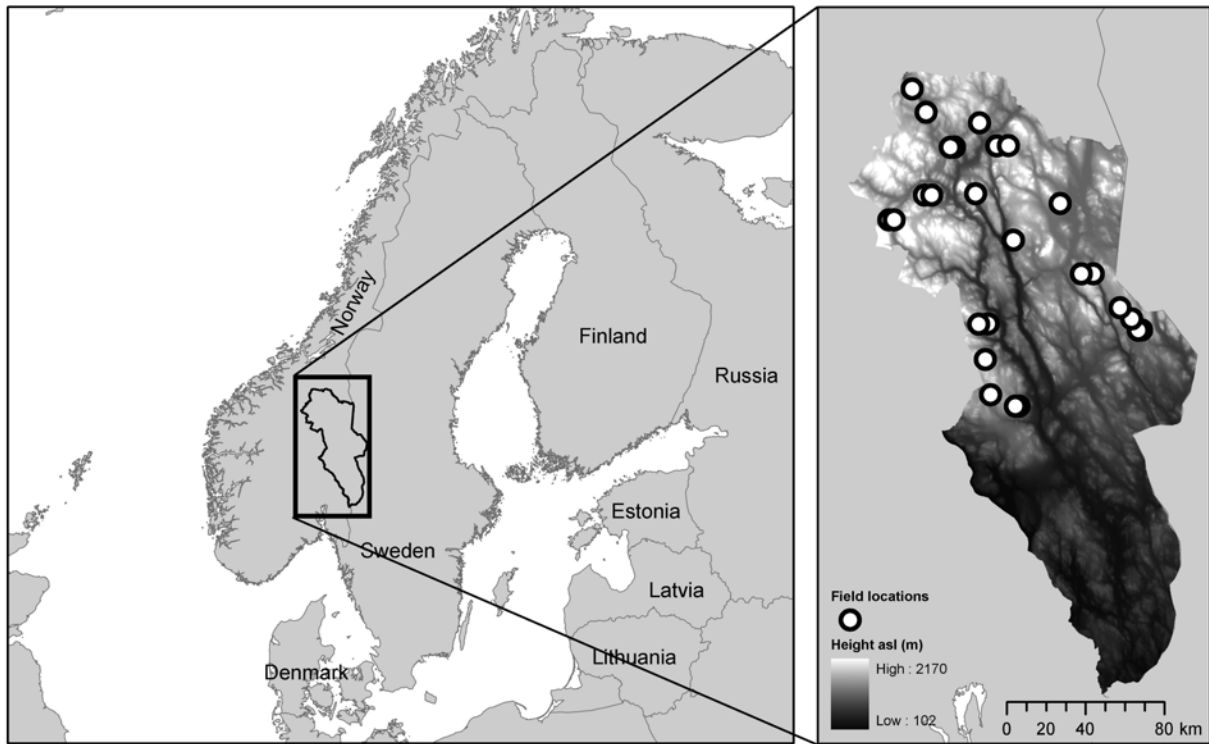
684 Table 3. Error matrix and accuracy measures of the class map created using logistic regression  
 685 and alpha-cuts.

686

	<b>Reference</b>			Sum	User's accuracy
	Forest	Subalpine zone	Alpine		
<b>Calibration dataset:</b>					
Forest	126	19	5	150	84.0
Subalpine zone	61	68	81	210	32.4
Alpine	7	22	254	283	89.8
Sum	194	109	340	643	
Producer's accuracy	64.9	62.4	74.7		
Overall accuracy					69.7
Kappa					0.53
<b>Test dataset:</b>					
Forest	274	55	25	354	77.4
Subalpine zone	115	133	161	409	32.5
Alpine	7	47	495	549	90.2
Sum	396	235	681	1312	
Producer's accuracy	69.2	56.6	72.7	0	
Overall accuracy					68.8
Kappa					0.52

687

688



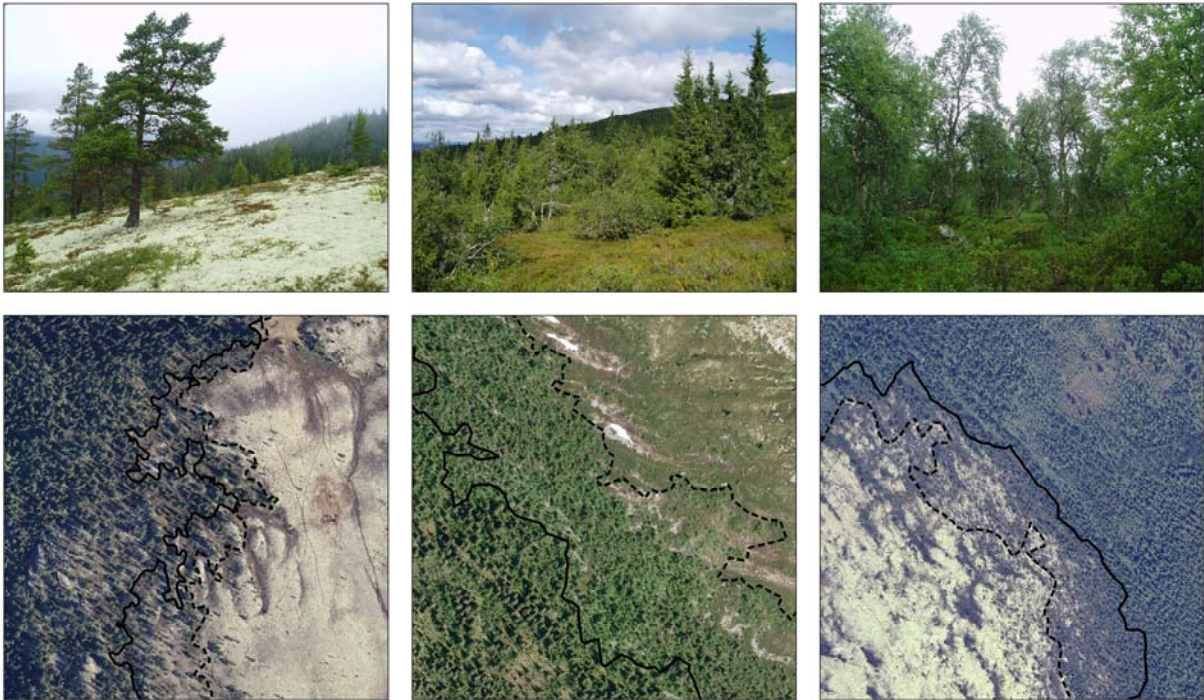
689

690

691 Fig. 1. Study area and field locations.

692

693

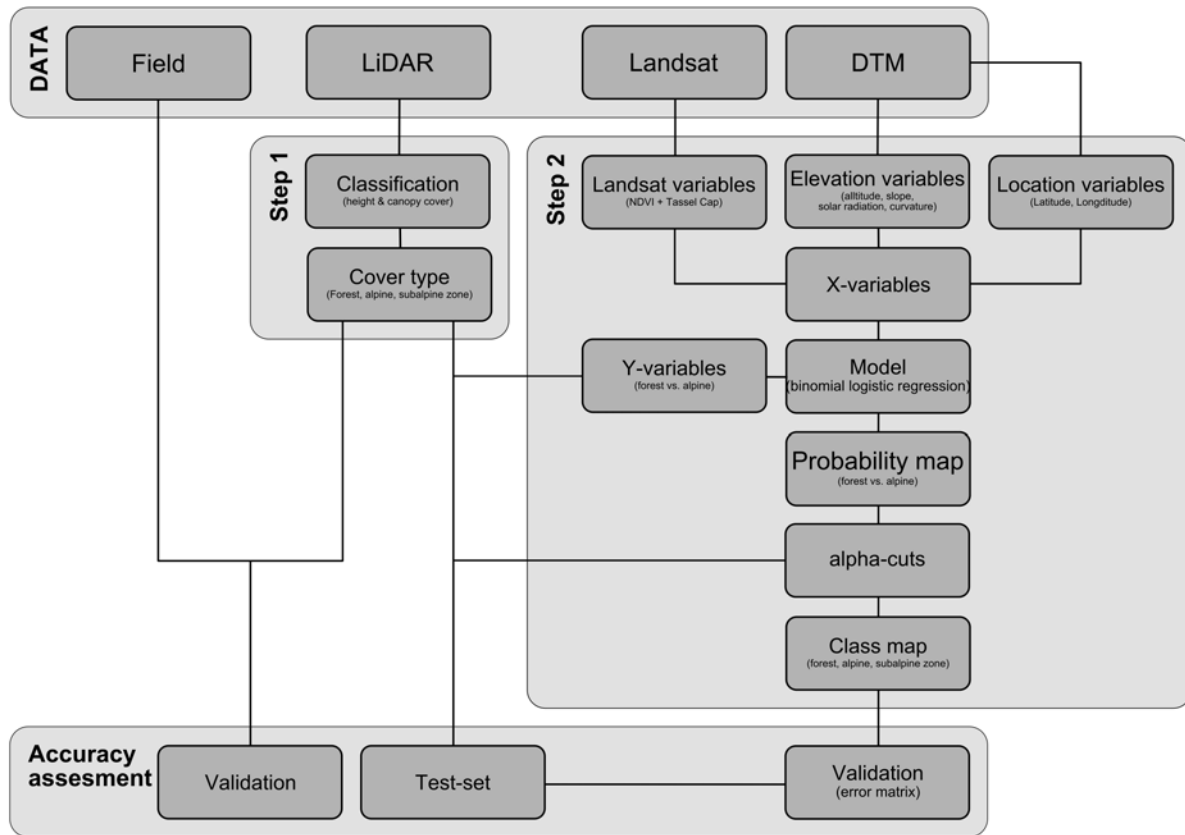


694

695

696 Fig.2. Examples of three sites with ground photo and orthophotos showing tree line (black dashed  
697 line) and forest line (black line). Sites from left; Heimrabben – Lichen-pine forest, Danseren –  
698 Vaccinium-spruce forest (birch at tree line), and Bjørnsjøklettan – Lichen-birch forest.

699

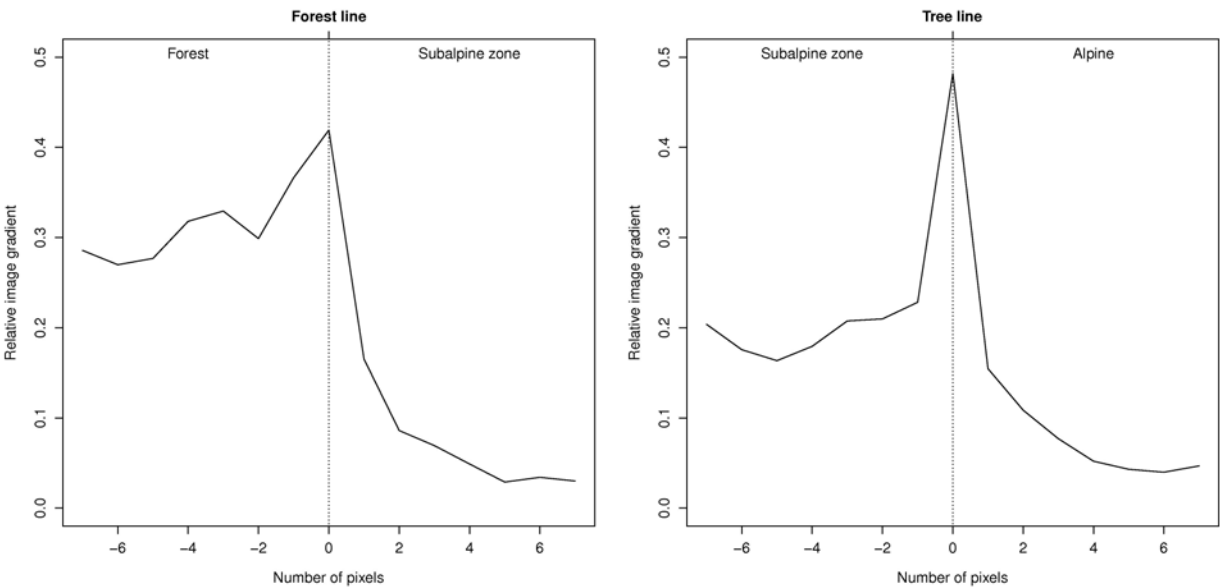


700

701

702 Fig. 3. Flow chart summarizing input data, analysis and accuracy assessment.

703



704

705

706

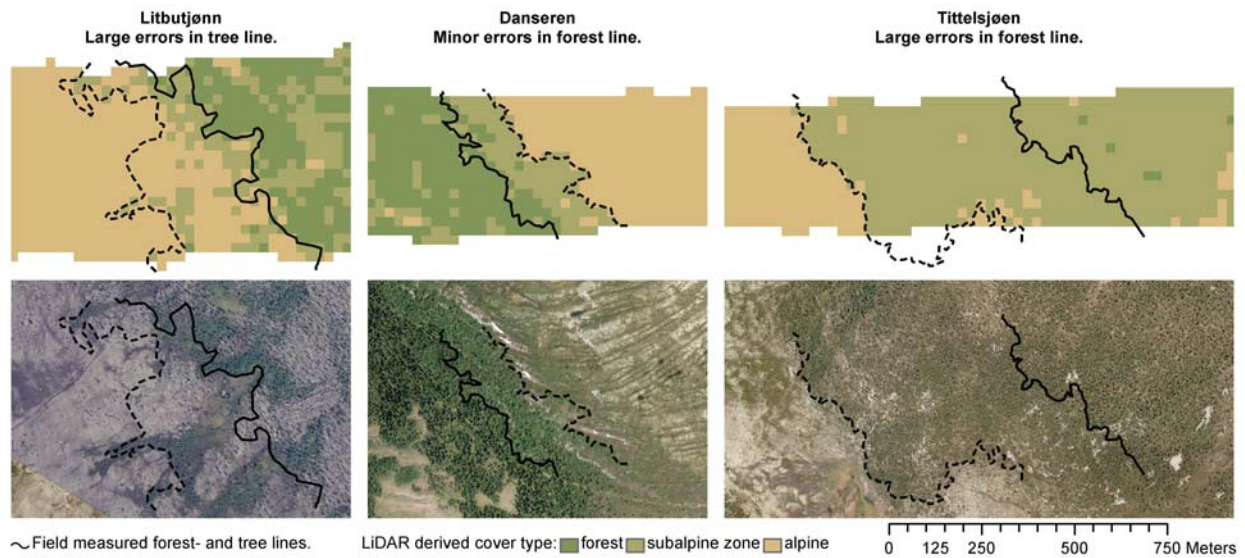
707

708

Fig. 4. Results of the accuracy assessment of the cover type classification from LiDAR. The average image gradient values (Eq. 3) for different distances from the field measured forest (left) and tree lines (right). The field measured forest and tree lines appear as vertical dotted lines.

709

710



711

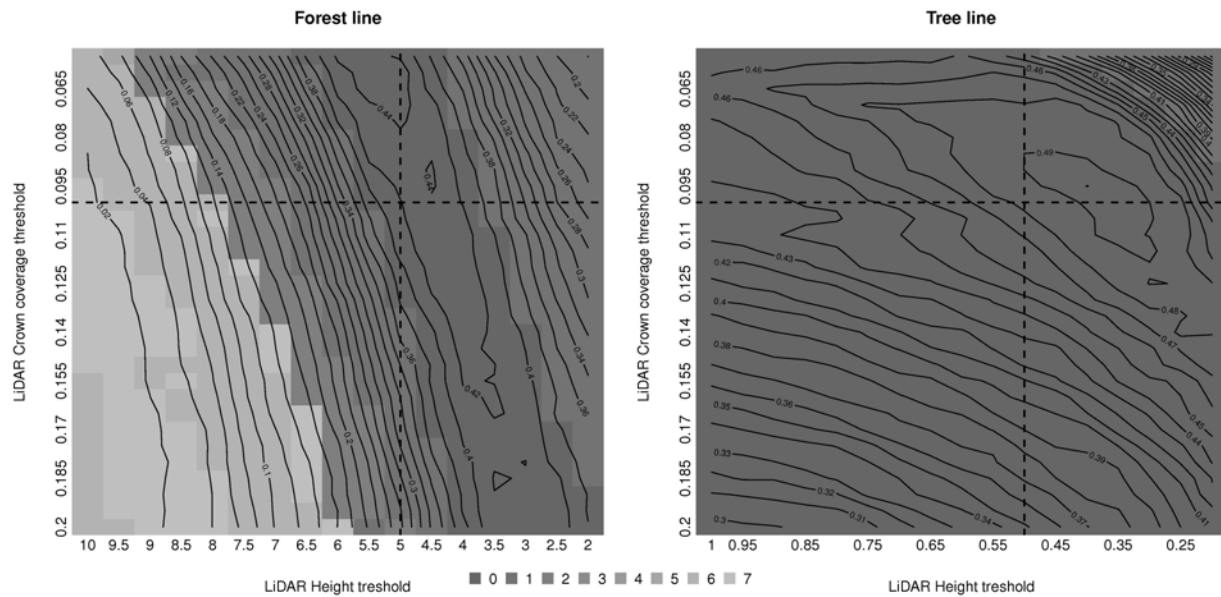
712

713 Fig. 5. Examples of the cover type classification from LiDAR (above). For comparison

714 orthophotos are display below. Forest and tree lines appear on both cover type classification and

715 on orthophotos as black lines.

716

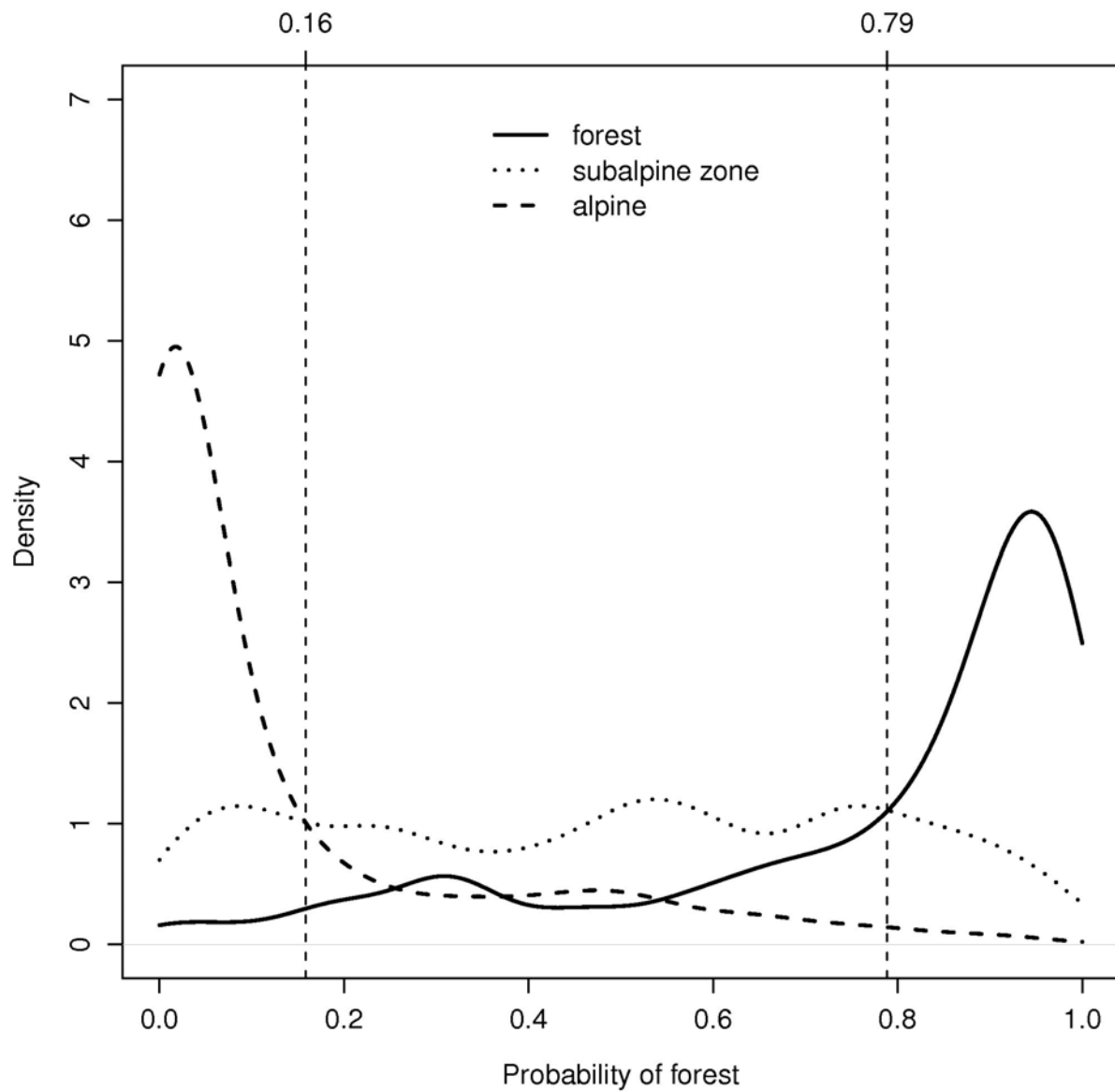


717

718

719 Fig. 6. Results of the sensitivity analysis where different height (x axis) and canopy thresholds (y  
 720 axis) are used in the LiDAR classification of cover types (forest, subalpine zone and alpine). The  
 721 contours represent average image gradient values (Eq. 3) at the field measured forest (left) and  
 722 tree lines (right). The distance from the highest image gradient value (Eq. 3) to field measured  
 723 forest and tree lines are represented by the number of pixels offset in gray scale from 1 to 7. The  
 724 dashed lines represent the values initially used in the study.

725



726

727 Fig. 7. The probability density functions for forest, alpine and subalpine zones used to set alpha-  
 728 cuts. The resulting alpha-cuts are displayed as vertical lines.